DESIGN AND EXPERIMENT OF A DRAG-REDUCTION DIGGING SHOVEL FOR PEANUT HARVESTERS IN SALINE-ALKALI SOIL

. 盐碱地花生收获机减阻挖掘铲的设计与试验

Pengcheng JI ¹⁾, Dongwei WANG ^{3,4)}, Farid Eltom ABDALLAH^{2,4)}, Yu TIAN⁴⁾, Abouelnardar SALEM⁴⁾, Huili ZHANG ^{*1)}, Haipeng YAN ⁴⁾

1)Qingdao Agricultural University/ China

²⁾National Center of Technology Innovation for Comprehensive Utilization of Saline-Alkali Land/ China
³⁾Dongying Institute of Efficient Agricultural Technology for Saline-Alkali Land, Qingdao Agricultural University/ China
⁴⁾Academician Workstation of Agricultural High-tech Industrial Area of the Yellow Rive Delta/ China
Tel: +86 13605424499; E-mail: zhhuili73@163.com
Corresponding author: Huili Zhang

DOI: https://doi.org/10.35633/inmateh-77-54

Keywords: Dung Beetle Head, Saline-Alkali Soil, Bionic Digging Shovel, Discrete Element Method

ABSTRACT

To address the challenges of difficult soil penetration and high digging resistance encountered by peanut harvesters in saline-alkali soils due to compaction, this study designed a drag-reducing digging shovel for peanuts in such environments, using the dung beetle head as a bionic prototype and incorporating agronomic requirements. Basic physical parameters of the saline-alkali soil were calibrated, and Bonding-model bond parameters were configured to establish a discrete element model of the soil-root system. The Hertz-Mindlin with JKR contact model was selected as the discrete element simulation model for the soil. A 3D scanner was employed to capture the morphology of the dung beetle, obtaining its precise three-dimensional model. The curve equation of the bionic digging shovel was determined, and its 3D model was constructed. Comparative simulation tests between the bionic and conventional digging shovels were conducted, during which particle flow velocities were tracked and their vector distributions analyzed to elucidate the drag reduction mechanism. Furthermore, by comparing the resistance forces acting on the conventional and bionic shovels at speeds of 0.4 m/s, 0.6 m/s, and 0.8 m/s, drag reduction rates of 4.82%, 3.03%, and 3.85%, respectively, were achieved for the bionic shovel. These results validate the accuracy of the mechanical model and the rationality of the bionic structural design.

摘要

针对当前花生收获机挖掘铲在盐碱地工作时,由于盐碱地土壤板结导致花生收获机械挖掘部件入土困难、挖掘阻力大等问题,本文以蜣螂头部为研究对象,结合农艺要求,设计了一款盐碱地花生减阻挖掘铲,通过对盐碱地土壤进行进本物理参数标定,设置 Bonding 键参数建立三七根茎的离散元模型。选用 Hertz-Mindlin with JKR模型作为土壤的离散元仿真模型。利用三维扫描仪对蜣螂进行扫描,获取蜣螂的三维模型。确定仿生挖掘铲的曲线方程,并建立仿生挖掘铲的三维模型。通过开展仿生挖掘铲与普通挖掘铲的仿真对比试验,并对颗粒的流速进行追踪,分析颗粒流速的矢量分布明晰了挖掘铲的减阻机理。再通过对比普通挖掘铲与仿生挖掘铲在0.4m/s、0.6m/s、0.8m/s 的速度下挖掘铲所受的阻力大小。得到仿生挖掘铲在这三个速度下的减阻率分别为4.82%、3.03%、3.85%。验证了挖掘铲力学模型构建准确,仿生结构设计合理。

INTRODUCTION

China maintains an annual peanut planting area of approximately 46,660 km², ranking second globally, with a production output of about 16.5 million tons, the highest worldwide. Due to their superior quality, peanuts have become a highly competitive oilseed crop for China in the international market (Wang., 2018). Peanuts also exhibit a degree of salt-alkali tolerance. Under appropriate cultivation management, they can achieve reasonable yields in saline-alkali soils, offering a new pathway for agricultural utilization of such land (Xian et al., 2022). However, during the harvesting process, mechanical digging components encounter difficulties penetrating the soil due to problems like compaction and increased hardness caused by high salinity and alkalinity. This can easily lead to issues such as a high rate of missed peanut plants during digging and severe pod loss. As a result, the efficiency and quality of the peanut harvest are compromised.

In the field of modern agricultural machinery research, bionic design and optimization techniques based on the Discrete Element Method (DEM) are increasingly emerging as cutting-edge and focal technologies (Zeng et al., 2021). Significant research has been conducted domestically and internationally on equipment design and improvement. In 1981, experiments analyzing the dynamic changes in operational resistance during soil cutting by shovel blades revealed a significant linear correlation between resistance and blade width, and a nonlinear relationship with digging depth (Spekto, 1981). Asghar et al., (2014), conducted an improved study on the rectangular blades of peanut harvesters. He optimized the cutting action of the blades and redesigned the original blade into a structure with three sharp, notch-free blades. Practical verification showed that the improved blades significantly increased the digging efficiency of the peanut harvester to 89.31% while effectively reducing the digging loss rate to 5.55%. Awuah, Emmanuel et al., (2014), proposed a technical scheme of blade vibration based on potato harvesters. This scheme generated high-frequency vibration of the digging shovel, which greatly weakened the reaction force of soil on the shovel body, enhanced the soil crushing effect, and significantly improved the overall efficiency of the harvester.

Bao Jianlun, (2021), designed a self-sharpening potato digging shovel with bionic characteristic curves. Taking rabbit incisors as the bionic prototype and combining the design of traditional potato digging shovels, he adopted bionic research methods and integrated the extracted bionic curves. Comparative analysis indicated that the bionic potato digging shovel was relatively superior to existing ordinary flat shovels in reducing resistance and self-sharpening effect. Wang Hengtai et al., (2014), addressed the problem that digging resistance restricts the development of root and tuber Chinese medicinal material harvesting machinery. Based on the toe structure of mole crickets, a bionic digging shovel was designed. Finally, soil bin and field tests were conducted to detect the resistance reduction effect and digging performance of the shovel, and the results showed that the bionic digging shovel had a certain resistance reduction effect compared with the flat shovel. Xia Chao et al., (2024), designed a digging shovel by fitting the contour curve of scallop shells. Comparison of simulation results between the bionic digging shovel and the ordinary one proved that the bionic shovel had better resistance reduction performance. Bao Dianling et al., (2024), designed a sweet potato digging shovel inspired by the morphology of golden cicadas, which demonstrated effective drag-reduction performance and also reduced the sweet potato breakage rate to a certain extent. Cao Chengmao et al., (2023), tackled the problem of high digging resistance during the harvesting of Peucedanum praeruptorum Dunn. Based on the Mohr-Coulomb theory, they selected the shark dorsal fin structure as the bionic shovel protrusion, obtained 3D models of shark dorsal fins and *Peucedanum praeruptorum Dunn* rhizomes through 3D scanning, and established a discrete element composite model of the bionic shovel, Peucedanum praeruptorum Dunn rhizomes, and soil. Comparison between discrete element simulation and soil bin tests showed that the digging resistance was reduced, meeting the harvesting requirements of Peucedanum praeruptorum Dunn. Li Junwei et al., (2023), aimed at the problems of high digging resistance and high energy consumption of potato digging shovels in heavy black soil areas. A bionic corrugated drag-reducing digging shovel was designed based on the membranous leaf sheath of cogongrass roots. Discrete element simulation and soil bin tests verified that the bionic digging shovel had good resistance reduction performance.

Based on the discrete element method and controlled experiments, this study presents the design of a bionic digging shovel inspired by the head structure of the dung beetle. Theoretical mechanical analysis was conducted on the bionic shovel, and simulation tests were carried out to validate its drag reduction performance.

DETERMINATION OF BASIC SOIL PHYSICAL PARAMETERS

Peanut cultivation typically employs ridge tillage as an agronomic requirement, generally implemented in a double-row seeding pattern per ridge. The ridge height ranges from 15 to 20 cm, with inter-ridge spacing of 75 to 85 cm (*Cui., 2020*). Saline-alkali soils usually exhibit a heavy texture and strong cohesion between soil particles. During operation, the shovel surface experiences significant resistance due to these soil conditions. The determination of basic physical parameters of the cultivated soil directly influences the establishment of discrete element models for saline-alkali soils.

Soil Density Determination

Using the five-point sampling method, a cutting ring was vertically pressed into the soil to collect an undisturbed sample. The sample ends were trimmed flat, sealed to prevent moisture loss, and the total mass of the ring and soil was measured with an electronic balance. The empty cutting ring mass was 165 g, and the test was repeated five times to obtain an average value.

Soil Moisture Content Test

Soil moisture content was determined using a DHQ-9075SA drying oven (Shanghai Yiheng). Samples in aluminum boxes were dried at 105°C for 8 hours, cooled to room temperature, and then weighed. The test was repeated five times, with the average value taken as the final moisture content.



Fig. 1- Soil Moisture Content Test

Soil Triaxial Shear Test

The critical shear stress of soil was determined using a TSZ-1 strain-controlled triaxial apparatus (Nanjing Soil Instrument Factory), complying with GB/T 15406-94. Testing followed GB/T 50123-2019, applying sequential confining pressures of 100, 200, 300, and 400 kPa with axial loading at 1.5 mm/min until specimen failure.

Particle Size Distribution Test

Soil particle composition was determined through sieve analysis using 0.25-3 mm standard test sieves. From a 2 kg dried sample, $500 \text{ g } (\pm 1 \text{ g})$ portions were sieved for 5 minutes. After five repeated tests, the mass fractions of particles in six size ranges $(0-0.25 \text{ to} \ge 3.0 \text{ mm})$ were measured as 5.00%, 8.00%, 10.97%, 24.00%, 23.55%, and 28.45%, respectively (Figure 2).



Fig. 2- Particle Size Distribution Test

The main physical parameters of the saline-alkali soil are as follows: average soil density 2.27×10³ kg/m³, soil moisture content 13.24%, and Poisson's ratio 0.32.

DISCRETE ELEMENT MODEL OF SOIL

EDEM provides novel approaches and methodologies for investigating complex dynamic behaviors exhibiting granular characteristics during agricultural field operations, such as soil layer separation, mixing, crack formation, and particle flow (Shi et al.,2017).

Based on soil adhesion characteristics and JKR contact theory, this study adopted the Hertz-Mindlin with JKR model as the discrete element simulation model for soil. The parameters were configured as follows: normal stiffness 1×10⁸ N/m, tangential stiffness 9×10⁷ N/m, JKR surface energy 6 J/m², bond radius 1.1 mm, restitution coefficient 0.31, static friction coefficient 0.56, and rolling friction coefficient 0.15 (Wang et al., 2024).

According to the soil particle size distribution and mass fractions, the median value of each particle size interval was used as the particle radius to configure particle factories, ensuring the simulated particle size distribution matched actual soil conditions. To balance computational accuracy and efficiency, the simulation particle diameter was set to 22 times the average soil particle diameter.

Furthermore, moisture enhances interparticle adhesion by participating in chemical bonding between soil particles (*Ding et al., 2017*), providing a theoretical basis for discrete element model selection.

Diameter distribution and mass fraction of soil particles in EDEM simulation

Diamotor distribution and mass resource of son particles in EDE in simulation			
True Particle Size	Simulation Particle Diameter	Particle Mass Fraction	
[mm]	[mm]	[%]	
0 ~ 1.0	11	23.97	
1.0 ~ 2.0	33	24.03	
2.0 ~ 3.0	55	23.55	
≥3.0	66	28.45	

To improve efficiency and reduce the simulation duration, a simulation region measuring 1200 mm × 500 mm × 280 mm was established, with reference to the agronomic requirements of peanut cultivation. The particle generation method was set to "Dynamic." The total number of particles generated by the particle factory was 393,000. Based on the classification in the table above, the quantities of soil particles were 332,000, 37,000, 13,000, and 11,000, respectively. The contact parameters between soil and the digging shovel were obtained by consulting relevant data (*Xia Chao et al., 2024*). The particle model and other related parameters were set according to Table 2. The resulting discrete element model is shown in Fig. 3.

Digger shovel-Soil contact parameters

Table 2

Table 1

Parameter Settings	Value	
Tool Poisson's Ratio	0.30	
Tool Density [kg/m³]	7865	
Tool Shear Modulus [Pa]	7.9×10 ⁹	
Tool-Soil Coefficient of Restitution	0.16	
Tool-Soil Rolling Friction Coefficient	0.20	
Tool-Soil Sliding Friction Coefficient	0.50	

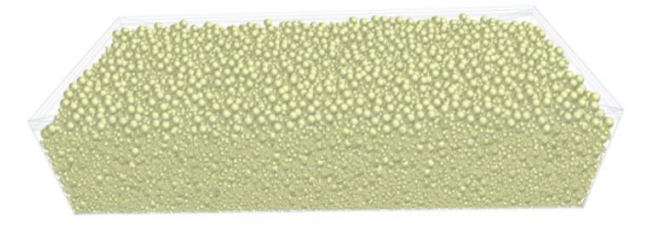


Fig. 3- Saline-alkali soil discrete element model

DESIGN OF THE BIONIC EXCAVATION SHOVEL STRUCTURE

In nature, animals have evolved specialized anatomical structures to adapt to their environments, which also provides insights for addressing challenges in agricultural production. For instance, Tian Kunpeng et al. successfully designed an innovative bionic cutting blade by mimicking the structural features of the mandibular cutting teeth of longhorn beetles (*Tian et al., 2017*). Similarly, Xiao Maohua et al. developed a rotary tiller blade inspired by the forelimb claws of the oriental mole cricket (*Xiao et al., 2021*).

The Soil-Cutting Mechanism of the Dung Beetle Head

It is assumed that the dung beetle moves along the OY direction, as illustrated in Fig. 4.

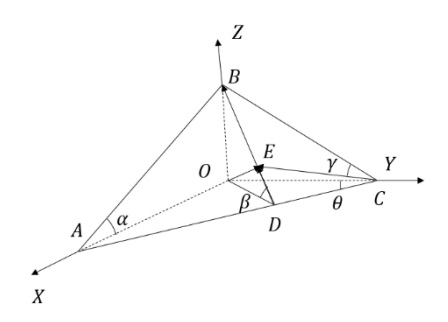


Fig. 4- Dung beetle head soil cutting mechanism

The trihedral wedge requires significantly less horizontal force when moving along its tip direction (OY-axis) compared to perpendicular motion (*Wu et al., 2019*). Tip-direction movement generates a slip-cutting effect with non-perpendicular blade engagement, reducing resistance through material tearing rather than crushing. In contrast, perpendicular motion produces vertical chopping that must overcome the material's full compressive strength, resulting in higher resistance.

3D Modeling of the Dung Beetle Head

The body of the dung beetle is predominantly black. To avoid color conflict with the background that could interfere with subsequent scanning, the beetle was coated in white. A Zhongce Technology OPSCAN S500D fully automatic 3D scanning and detection system was used to perform the scan. The result is shown in Fig. 5.

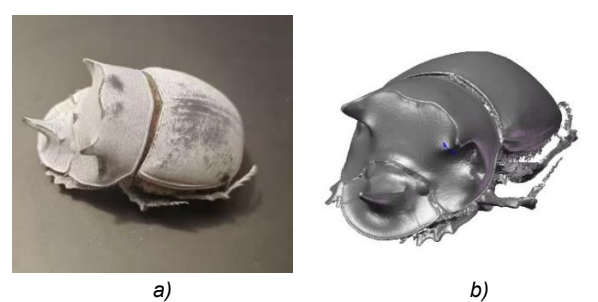


Fig. 5– 3D Scanned Model of a Dung Beetle
a) Actual Dung Beetle Specimen; b) 3D Model of the Dung Beetle

Geometric Data Capture of Beetle Head

The obtained 3D model of the dung beetle was imported into SolidWorks software. The model was then adjusted to an optimal orientation. Within the menu bar, the Autotrace plugin was selected and activated to generate the contour lines of the dung beetle. The specific result is illustrated in Fig. 6.

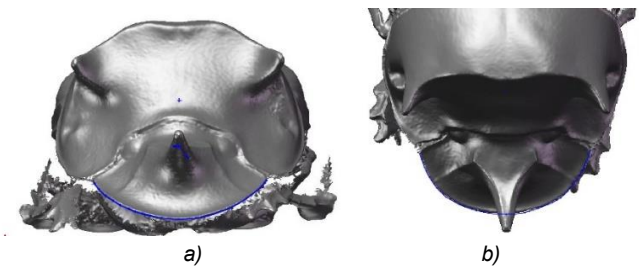


Fig. 6–Head Contour Diagram of a Dung Beetle
a) Contour Curve of Front View; b) Contour Curve of Top View

The curve was fitted using MATLAB. As shown in Table 3, the fitting accuracy improves with increasing polynomial order, with cubic and quartic polynomials showing significantly higher accuracy than quadratic. When accuracy requirements are met, lower-order equations should be prioritized to simplify the bionic design process.

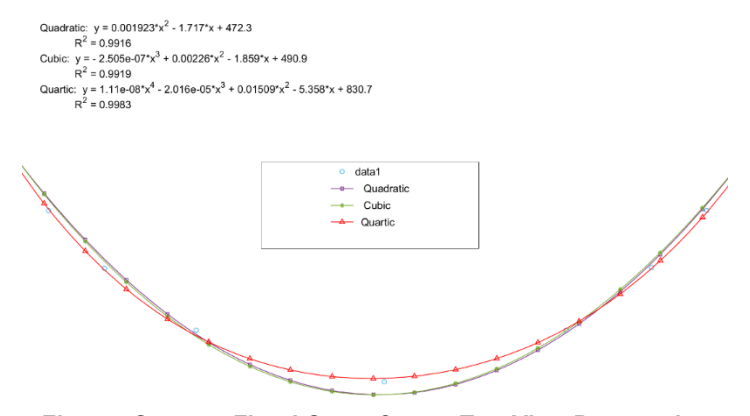


Fig. 7 - Contour-Fitted Curve from a Top-View Perspective

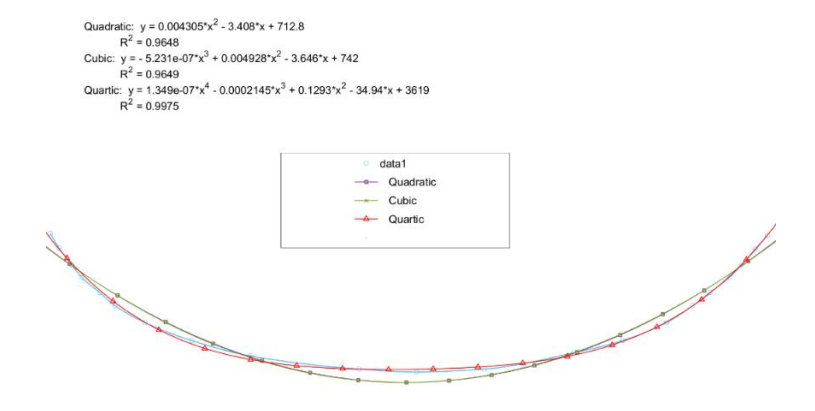


Fig. 8 - Contour-Fitted Curve from a Front-View Perspective

Correlation coefficient of contour curve equation R2

Table 3

Curve-Fitting Model	Correlation Coefficient R ² for Top View Equation	Correlation Coefficient R ² for Front View Equation
Second-Order Polynomial	0.9916	0.9648
Third-Order Polynomial	0.9919	0.9649
Fourth-Order Polynomial	0.9983	0.9975

The final selected fitting equation for the top view is a quartic polynomial, namely:

$$y = 1.11e^{-08}x^4 - 2.016e^{-05}x^3 + 0.01509x^2 - 5.358x + 830.7$$
 (1)

The fitting equation for the top view is a quartic polynomial, expressed as:

$$y = 1.349e^{-07}x^4 - 0.0002145x^3 + 0.1293x^2 - 34.94x + 3619$$
 (2)

FORCE ANALYSIS OF THE BIONIC SHOVEL

Mechanism Analysis of Trihedral Wedge Excavation

Analysis revealed that the structure of the digging shovel conforms to the mechanical principle of the trihedral wedge (*Zhang et al., 2024*). Based on this principle, the three-dimensional model of the digging shovel was simplified, and a mechanical model diagram of the shovel was established, as shown in the figure.

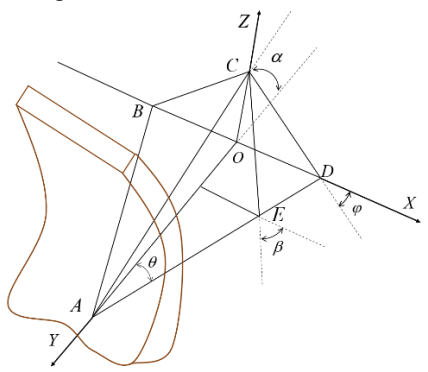


Fig. 9 - Principle analysis of excavating shovel wedge

 α - soil-cutting load Angle, [°];

 β - soil-cutting wedge angle, [°];

 θ - shovel surface inclination angle, [°];

 φ - soil-entry angle, [°];

 l_{AO} - distance between points A and O, [mm];

 l_{co} - distance between points C and O, [mm];

 $l_{\scriptscriptstyle DO}$ - distance between points D and O, [mm];

 l_{EO} - distance between points E and O, [mm].

Based on the force relationship diagram, the relationship between the various wedge angles can be derived as:

$$\begin{cases}
\tan \alpha = \frac{l_{CO}}{l_{AO}} \\
\tan \beta = \frac{l_{CO}}{l_{EO}} \\
\sin \theta = \frac{l_{EO}}{l_{AO}}
\end{cases} \tag{3}$$

$$\begin{cases}
\tan \theta = \frac{l_{DO}}{l_{AO}} \\
\tan \varphi = \frac{l_{CO}}{l_{DO}}
\end{cases} \tag{4}$$

Combining equations (3) and (4) yields:

$$\tan \alpha = \tan \beta \tan \theta \tag{5}$$

In summary, the soil-cutting load angle α is directly influenced by the soil-cutting wedge angle β and the shovel surface inclination angle θ . From the perspective of the trihedral wedge's mechanism of action on soil, the main factors affecting digging resistance include the soil-cutting load angle α , the shovel surface inclination angle θ , and the soil-entry angle φ . By adjusting the shovel surface inclination angle θ , the magnitude of the soil-cutting load angle α can be actively controlled. When α is relatively small, the cutting edge can penetrate the soil at a "sharper" angle, more readily inducing slip-cutting and thereby reducing resistance.

Force Analysis on the Digging Shovel Surface

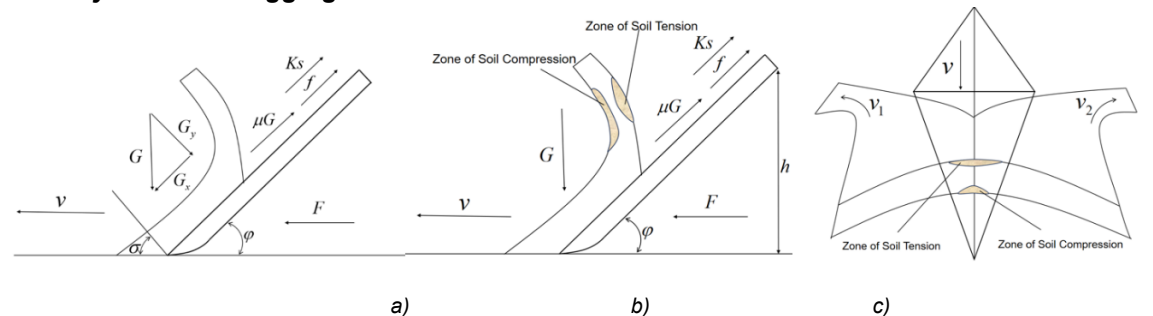


Fig. 10- Force Analysis on the Digging Shovel Surface

a) Force Analysis on the Surface of an Excavation Shovel; b) Analysis of Lateral Forces on an Excavation Shovel; c) Force Analysis on the Front Face of the Excavating Shovel

Based on the lateral mechanical equilibrium equation of the digging shovel shown in the figure:

$$F = G\sin\varphi + (\mu G + KS + f)\cos\varphi \tag{6}$$

Horizontal force equilibrium equation is:

$$G_{v}\cos\sigma + (f + KS + \mu G_{v})\cos\varphi + KS\sin\sigma - G_{x}\cos\varphi - \mu G_{v}\cos\sigma = 0$$
 (7)

Vertical force equilibrium equation is:

$$G + (KS + f + \mu G_v)\sin\varphi + KS\cos\sigma + \mu G_v\sin\varphi - G_v\sin\sigma = 0$$
 (8)

By combining equations (6) to (8), the resistance equation for the digging shovel moving through soil is derived:

$$F = \frac{G}{Z} + \frac{f + KS}{Z(\sin \sigma + \mu \cos \sigma)} + \frac{KS}{Z(\sin \varphi + \mu \cos \varphi)}$$
(9)

where:

$$Z = \frac{\cos \varphi - \mu \sin \varphi}{\sin \varphi + \mu \cos \varphi} - \frac{\cos \sigma - \mu_1 \sin \sigma}{\sin \sigma + \mu_1 \cos \sigma}$$
(10)

F - digging resistance, [N];

G - gravity of root-soil mixture, [N];

K - soil adhesion, [MPa];

f - pure cutting force, [N];

S - working contact area of digging shovel, [N];

 μ - internal soil friction factor

 G_x - normal load on digging shovel, [N];

 G_y - lateral load on digging shovel, [N];

 σ - front failure surface inclination angle, [°];

h - digging depth, [mm];

 $\mu_{\!\scriptscriptstyle 1}$ - soil-metal friction factor

Z - constant.

Through analysis of the mechanical model established for the root-soil mixture and digging shovel during the excavation process, it was found that the geometric structural parameters of the shovel, operational parameters, and soil physical properties are the main factors influencing the digging resistance. By taking the partial derivative of the resistance force F with respect to these variables, the optimal values of the soil-entry angle ϕ and the resistance angle σ that minimize the resistance can be determined.

$$\begin{cases} \frac{\partial F}{\partial \sigma} = -\frac{KS + f}{Z(\sin \sigma + \mu \cos \sigma)^2} (\cos \sigma - \mu \sin \sigma) = 0\\ \frac{\partial y}{\partial x} = -\frac{KS}{Z(\sin \varphi + \mu \cos \varphi)^2} (\cos \varphi - \mu \sin \varphi) = 0\\ \left(0 \le \sigma \le \frac{\pi}{2}, 0 \le \varphi \le \frac{\pi}{2}\right) \end{cases}$$
(11)

According to the formula, when the soil-entry angle φ and the resistance angle σ approach 45°, the digging resistance of the shovel is minimized.

SIMULATION TEST

To minimize experimental error, the flat shovel was designed with identical dimensions to the bionic shovel. The flat shovel was designed with the following dimensions (length \times width \times thickness): 131 mm \times 66.5 mm \times 5 mm, a tip half-angle of 88°, a working width of 346.5 mm, and an inter-blade gap of 73.5 mm. The flat shovel was modeled using SolidWorks software, with the result shown in Figure 11.

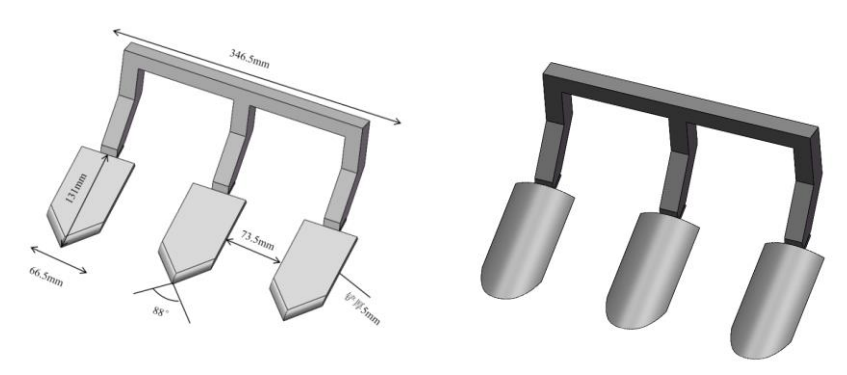
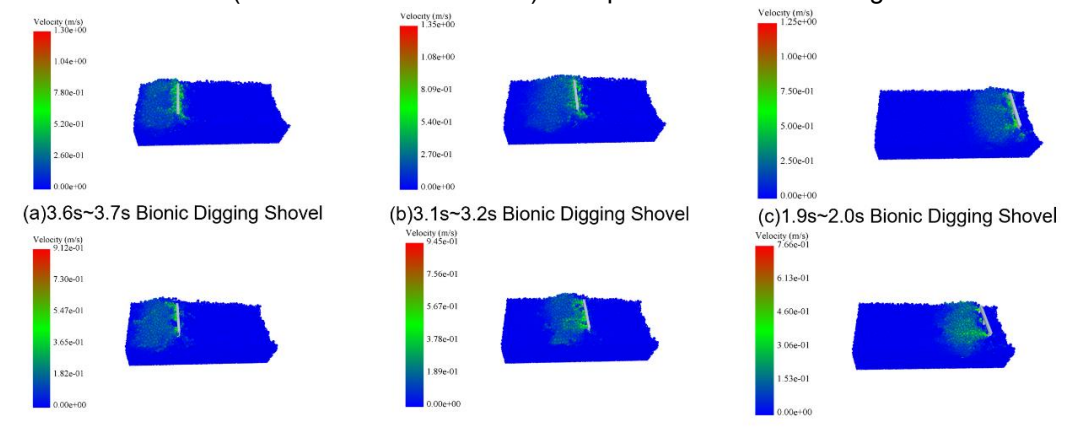


Fig. 11 - 3D Diagrams of Conventional Digging Shovel and Bionic Digging Shovel

Simulation Test of the Digging Shovel

A simulation modeled the digging shovel's movement in soil. During 0-1.2 s, soil-shovel parameters were configured, bonds established, and particles generated. Bionic and flat shovel STL models were imported into EDEM 2022. Based on peanut harvesting requirements, the depth was set to 180 mm and entry angle to 27°.

Three test groups were established with linear translation speeds of 0.4, 0.6, and 0.8 m/s. The total motion duration was 2.8 s (1.2-4.0 s simulation time). The process is shown in Figure 12.



(d)3.6s~3.7s Conventional Digging Shovel (e)3.1s~3.2s Conventional Digging Shovel (f)1.9s~2.0s Conventional Digging Shovel

Fig. 12- Comparison Diagram from Simulated Excavation Shovel Tests

Comparison of Soil Particle Velocities

Simulation data was exported via EDEM post-processing and imported into Origin for analysis, yielding the 0-3.7 s time-velocity curve (shown). The average X-axis velocities for the conventional and bionic shovels were 0.0058 m/s and 0.0074 m/s, respectively. During the start-up phase (1.2-2.0 s), X-axis velocity began rising; it stabilized during the steady-state phase (2.0-3.7 s). The bionic shovel performed better along both Y/Z axes: Y-axis average velocity 0.0011 m/s (conventional: 0.0008 m/s), Z-axis average velocity 0.0080 m/s (conventional: 0.0072 m/s). During 1.2-1.7 s, the bionic shovel's Y-axis velocity increased significantly faster, as its unique structure guides orderly lateral slippage of soil particles, effectively reducing accumulation resistance. The Z-axis curve showed notable changes during 1.2-1.7 s due to upward soil movement along the shovel surface, stabilizing after 1.7 s. Comprehensive three-axis velocity analysis confirms the bionic shovel's superior soil guidance, enhanced flowability, and demonstrated structural advantages in drag reduction.

Analysis of Digging Shovel Resistance

During the simulation of the digging process, both shovels (bionic and conventional) began moving and contacting the soil at 1.2 s, entering the excavation phase. As the operation progressed, the digging resistance on both shovels gradually increased. After 2.0 s, the resistance variation stabilized. To study the resistance values under different velocities, the average digging resistance within the time period of 1.2–4.0 s was calculated.

At the same velocity, given that the horizontal resistance of the bionic shovel is lower than that of the conventional shovel, the drag reduction rate of the bionic shovel can be calculated using Equation 12. The specific formula is as follows:

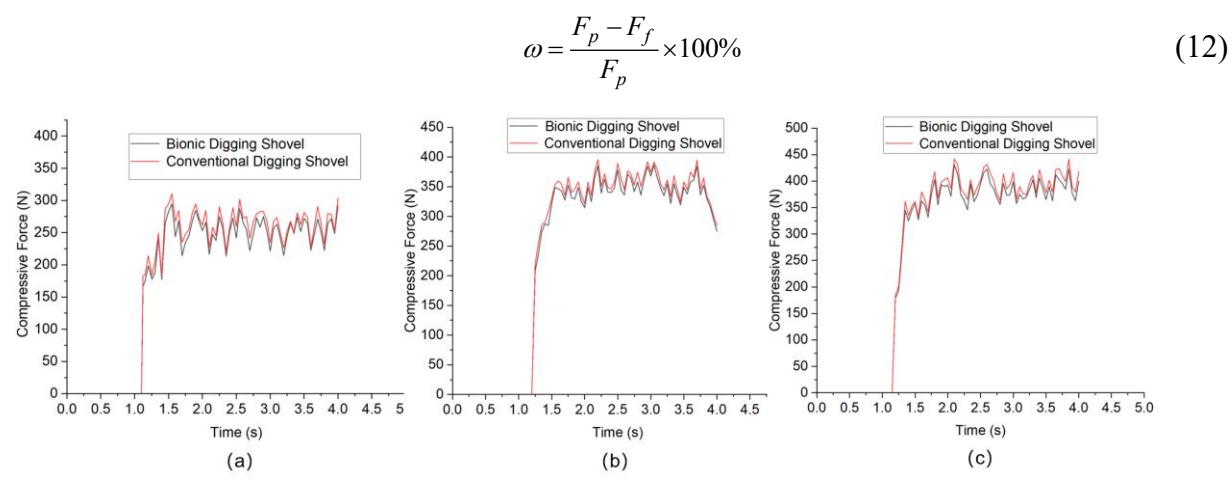


Fig. 13 – Comparison Diagram from Simulated Excavation Shovel Tests

a) Resistance Force on the Excavating Shovel at a Speed of 0.4 m/s; b) Resistance Force on the Excavating Shovel at a Speed of 0.6 m/s;

c) 18 Resistance Force on the Excavating Shovel at a Speed of 0.6 m/s

The resistance and drag reduction rate at a speed of 0.4m/s

Table 3

		_
Conventional Shovel / N	Bionic Shovel / N	Drag Reduction Rate / %
261.978	253.032	3.53
247.587	235.155	5.28
257.165	250.497	2.66
272.517	265.765	2.54
279.169	273.304	2.15
234.621	221.430	5.96
226.321	214.506	5.51
280.654	273.902	2.47
258.996	246.897	4.90
232.312	222.654	4.34
303.546	291.126	4.27
255.462	243.704	4.82
	261.978 247.587 257.165 272.517 279.169 234.621 226.321 280.654 258.996 232.312 303.546	261.978 253.032 247.587 235.155 257.165 250.497 272.517 265.765 279.169 273.304 234.621 221.430 226.321 214.506 280.654 273.902 258.996 246.897 232.312 222.654 303.546 291.126

The resistance and drag reduction rate at a speed of 0.6m/s

Table 4

	•		
Time / s	Conventional Shovel / N	Bionic Shovel / N	Drag Reduction Rate / %
2.0	314.461	321.011	2.02
2.2	385.165	395.504	2.68
2.4	339.987	346.112	1.08
2.6	335.285	344.633	2.78
2.8	357.787	374.461	4.60
3.0	367.675	374.670	1.90
3.2	334.778	344.553	2.92
3.4	335.567	345.687	3.02
3.6	357.257	374.348	4.87
3.8	352.676	364.654	3.39
4.0	275.357	384.354	3.27
Average	341.489	351.844	3.03

Table 5
The resistance and drag reduction rate at a speed of 0.8m/s

The resistance and drag reduction rate at a speed of violing				
Time / s	Conventional Shovel / N	Bionic Shovel / N	Drag Reduction Rate / %	
2.0	392.546	405.846	3.38	
2.2	374.264	385.654	3.04	
2.4	361.361	382.841	5.94	
2.6	422.987	439.549	3.98	
2.8	355.751	369.848	3.96	
3.0	398.748	416.176	4.29	
3.2	369.876	374.212	1.17	
3.4	405.654	421.464	3.89	
3.6	362.954	379.248	4.48	
3.8	384.498	398.984	3.76	
4.0	399.846	417.628	4.44	
Average	384.408	399.223	3.85	

Under identical operating conditions and at speeds of 0.4 m/s, 0.6 m/s, and 0.8 m/s, the drag reduction rates of the bionic digging shovel were 4.82%, 3.03%, and 3.85%, respectively. Among the three tested operating conditions, the most significant drag reduction effect was observed at the speed of 0.4 m/s, where the drag reduction rate was comparatively higher.

Analysis of the Digging Mechanism

To investigate the digging mechanism and better understand the causes of digging resistance, the working state of the digging shovel at 3.7 s was selected. Using the post-processing tool Analyst, the velocity vector diagram of soil particles was generated, as shown in Figure 11. In the diagram, the direction of the vector arrows directly indicates the movement direction of the soil particles, the length of the arrows corresponds to the magnitude of particle velocity, and the color variation represents trends in particle speed.

By combining the structure of the digging shovel and comparing the velocity vector directions and magnitudes of soil particles around the shovel at 3.7 s, the movement trends and states of particles in the vicinity of the shovel can be determined.

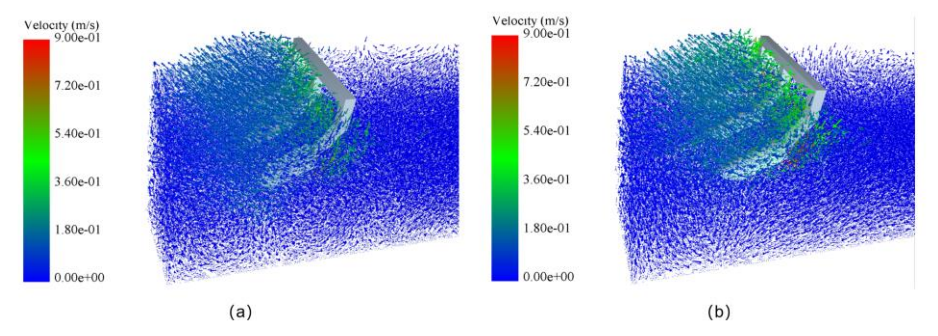


Fig. 14- Vector Diagram Illustrating Soil Particle Displacement

a) Velocity Vector Diagram of Soil Particles for the Conventional Flat Shovel; b) Velocity Vector Diagram of Soil Particles for the Bionic Digging Shovel

Soil particles near the edge of the digging shovel experience stronger disturbance. Particles in front of the shovel are subjected to a forward force and move along the X-axis, with their velocity direction aligned with the X-axis. The velocity direction of particles in the central region gradually shifts toward the Z-axis, and the resistance on the shovel transitions to the upper part of the shovel. At this stage, soil particles gradually accumulate, forming soil blockage. By analyzing the velocity vector distribution of soil particles, it can be observed that the resistance during shovel operation primarily originates from the forces exerted on the front and central parts of the shovel.

The bionic shovel demonstrates significantly higher soil particle flow velocity and more dispersed velocity distribution compared to the conventional flat shovel. This advantage originates from its comprehensively curved surfaces, which promote soil fragmentation, slippage, and rolling along all three axes, creating spatially divergent particle movement. This design enhances soil fluidity and diversion, reduces soil accumulation on the shovel surface, effectively minimizes blockage, and consequently improves operational efficiency through reduced resistance.

CONCLUSIONS

- 1. Based on the calibration of fundamental physical parameters of saline-alkali soil and combined with peanut cultivation agronomy, an accurate discrete element bonding model of the soil was established to prepare for comparative excavation simulation tests.
- 2. The three-dimensional model of the dung beetle was acquired, and the expression of the bionic design curve for its head was derived by fitting scattered points. The theoretical mechanical model of the digging shovel was developed and analyzed, and the 3D model of the bionic digging shovel was created using SolidWorks.
- 3. Comparative excavation simulation tests were conducted to evaluate soil particle velocities along the X, Y, and Z axes. By analyzing the three-axis velocity vector diagrams of soil particles, the drag reduction mechanism of the shovel was clarified. Through comparison of the resistance forces acting on the shovels, a drag reduction rate of 3.9% was obtained for the bionic digging shovel in the simulation tests. By comparing the excavation processes of the bionic and flat shovels, it was demonstrated that the bionic shovel surface, due to its curved structure, exhibits better soil guiding and drag reduction effects compared to the flat shovel.

ACKNOWLEDGEMENTS

The work was supported by the Development of Key Equipment for Intelligent Seeding in Saline-Alkal (WSR2024092). Development of Key Components for Efficient Tillage Equipment in Saline-Alkali Land (Y20240055). Innovation and Industrialization of Key Technologies for Combined Tillage-Seeding Equipment in Saline-Alkali Land (2024CGZH14).

REFERENCES

[1] Wang, B. (2018). Study on the Picking Mechanism and Screening Characteristics of a Four-Row Semi-Feeding Peanut Combine Harvester (四行半喂入花生联合收获摘果机理与筛选特性研究). Chinese Academy of Agricultural Sciences.

- [2] Xian, J. H., & Wang, J. Q. (2022). Effects of different planting patterns on peanut growth and soil properties in saline-alkali land (盐碱地花生不同种植模式对生长及土壤性质的影响). *Agricultural Engineering Technology*, Vol.42, No.02, pp.31–32. Beijing/China.
- [3] Zeng, Z. W., Ma, X., Cao, X. L., Li, Z. H., & Wang, X. C. (2021). Application status and prospects of discrete element method in agricultural engineering research (离散元法在农业工程研究中的应用现状和展望). *Journal of Agricultural Machinery*, Vol.52, No.04, pp.1-20. Beijing/China.
- [4] Spektor M. (1981). Principles of soil-tool interaction. *Journal of Terramechanics*, Vol.18, No.1, pp. 51-65. DOI: 10.1016/0022-4898(81)90017-3.
- [5] Asghar, Muhammad & Ghafoor, Dr. Abdul & Munir, Anjum & Iqbal, Muhammad & Choudhary, Manzoor (2014). Design Modification and Field Testing of Groundnut Digger. *Asian Journal of Science and Technology*. Vol.5, No.04, pp.389-394.
- [6] Awuah, E., Zhou, J., Liang, Z., Aikins, K. A., Gbenontin, B.V., Mecha, P., & Makange, N.R. (2022). Parametric analysis and numerical optimisation of Jerusalem artichoke vibrating digging shovel using discrete element method. *Soil and Tillage Research*, Vol.219, 105344.
- [7] Bao, J.L. (2021). *Design and Experiment of a Bionic Self-Sharpening Potato Digging Shovel* (仿生自磨 锐马铃薯挖掘铲的设计与试验). Jilin University.
- [8] Wang, H. T., Sun, W., Wang, J. X., & Zhao, H. (2023). Design and experiment of bionic digging shovel for root-type Chinese medicinal herbs (根茎类中药材仿生挖掘铲的设计与试验). *Journal of Gansu Agricultural University*, Vol.58, No.01, pp.243–250. Gansu/China.
- [9] Xia, C., Shang, S. Q., Wang, D. W., Liu, Y. G., He, X. N., Zhao, Z., ... & Zuo, B. Q. (2024). Design and experiment of bionic scallop peanut digging shovel (仿生扇贝花生挖掘铲的设计与试验). *Journal of Agricultural Mechanization Research*, Vol.46, No.03, pp.114–119. Heilongjiang/China.
- [10] Bao, D.L., Zhang, C.Y., Li, M., Yang, X.J., & Liu, X.W. (2024). Design and experiment of bionic cicada-inspired sweet potato digging shovel (基于仿生金蝉甘薯挖掘铲的设计与试验). *Journal of Heilongjiang University of Technology (Comprehensive Edition)*, Vol.24, No.09, pp.122–127. Heilongjiang/China.
- [11] Cao, C. M., Liu, Z. B., Ding, W. Y., Wu, M. Y., Zhang, X. C., & Qin, K. (2023). Design and experiment of bionic digging shovel for Ningqianhu (宁前胡仿生挖掘铲设计与试验). *Journal of Agricultural Machinery*, Vol.54, No.11, pp. 102–113. Beijing/China.
- [12] Li, J. W., Gu, T.L., Li, X. Y., Wang, Z. J., Hu, B., & Ma, Y. H. (2023). Analysis and experiment of bionic drag reduction characteristics of potato digging shovel in heavy black soil (黏重黑土条件下马铃薯挖掘铲仿 生减阻特性分析与试验). *Transactions of the Chinese Society of Agricultural Engineering*, Vol.39, No.20, pp.1-9. Beijing/China.
- [13] Cui, S.J. (2020). High-yield cultivation techniques of peanut in saline-alkali soil in Laizhou City(莱州市 盐碱地花生高产栽培技术). *Bulletin of Agricultural Science and Technology*, No.12, pp.259-261. Beijing/China.
- [14] Shi, L. R., Zhao, W. Y., & Sun, W. (2017). Contact model and parameter calibration for farmland soil particles in arid areas of Northwest China based on discrete element method (基于离散元的西北旱区农田 土壤颗粒接触模型和参数标定). *Transactions of the Chinese Society of Agricultural Engineering*, Vol.33, No.21), pp.181-187. Beijing/China.
- [15] Wang, D. W., Lu, T., Zhao, Z., Shang, S. Q., Zheng, S., & Liu, J. (2024). Calibration method of discrete element simulation parameters for cultivated layer soil in coastal saline-alkali land (滨海盐碱地耕作层土壤 离散元仿真参数标定方法). *Journal of Agricultural Machinery*, Vol.55, No.11), pp.240-249. Beijing/China.
- [16] Ding, Q. S., Ren, J., Adam, B. E., Zhao, J. K., Ge, S. Y., & Li, Y. (2017). Discrete element analysis of subsoiling process in wet sticky paddy soil (湿粘水稻土深松过程离散元分析). *Journal of Agricultural Machinery*, Vol.48, No.03, pp.38-48. Beijing/China.
- [17] Tian, K. P., Li, X. W., Shen, C., Zhang, B., Huang, J. C., Wang, J. G., & Zhou, Y. (2017). Design and experiment of bionic longhorn beetle cutting blade for hemp harvester (天牛仿生大麻收割机切割刀片设计与试验). *Transactions of the Chinese Society of Agricultural Engineering*, Vol.33, No.05, pp.56-61. Beijing/China.
- [18] Wu, N., Zhang, F., & Tong, J. (2009). Mechanical analysis of soil cutting resistance reduction by clypeus of Dung Beetle (臭蜣螂唇基切土减阻的力学分析). *Journal of Agricultural Machinery*, Vol.40, No.10, pp.207-210+222. Heilongjiang/China.

- [19] Xiao, M. H., Wang, K. X., Yang, W., Wang, W. C., & Jiang, F. (2021). Design and experiment of bionic rotary blade based on claw toe of oriental mole cricket (基于东方蝼蛄爪趾的仿生旋耕刀设计与试验). *Journal of Agricultural Machinery*, Vol.52, No.02, pp.55-63. Heilongjiang/China.
- [20] Zhang, Q., Liang, L. S., & Zhang, J. S. (2024). *Agricultural Machinery* (农业机械学). Chemical Industry Press. Beijing/China.